

Why LoRA Resists Label Noise: A Theoretical Framework for Noise-Robust Parameter-Efficient Fine-Tuning

Brady Steele¹

Abstract

Parameter-efficient fine-tuning methods like Low-Rank Adaptation (LoRA) have become the dominant paradigm for adapting large pretrained models. We present a theoretical framework explaining an underexplored property: LoRA’s inherent resistance to label noise. Our analysis reveals three key insights. First, we prove that rank- r LoRA cannot memorize all possible label assignments once the sample size exceeds $\mathcal{O}(r(d+k-r))$, limiting its capacity to fit arbitrary noise. Second, we derive an optimal rank balancing approximation bias and noise-induced variance, showing it decreases with noise rate. Third, we establish temporal separation: clean patterns are learned early while noise memorization occurs later. We propose RACT (Rank-Aware Curriculum Training), leveraging rank discrepancy for noise detection. Experiments validate our predictions, with RACT achieving 91.1% F1 for noise detection on AG News while maintaining 91.46% accuracy, competitive with baselines that lack noise detection capability.

1. Introduction

The success of large pretrained models across natural language processing (Devlin et al., 2019; Brown et al., 2020), computer vision (Dosovitskiy et al., 2021; Radford et al., 2021), and multimodal domains (OpenAI, 2023) has established transfer learning as the default paradigm for machine learning practitioners. However, full fine-tuning of models with billions of parameters presents significant computational and memory challenges. Parameter-efficient fine-tuning (PEFT) methods address this by updating only a small subset of parameters while freezing the pretrained backbone (Houlsby et al., 2019; Lester et al., 2021; Hu et al., 2022).

¹Georgia Institute of Technology, Atlanta, GA, USA. Correspondence to: Brady Steele <bsteele45@gatech.edu>.

Submitted to ICML 2026.

Among PEFT methods, Low-Rank Adaptation (LoRA) (Hu et al., 2022) has emerged as particularly popular due to its simplicity and effectiveness. LoRA parameterizes weight updates as the product of two low-rank matrices $\Delta W = BA$, where $B \in \mathbb{R}^{d \times r}$ and $A \in \mathbb{R}^{r \times k}$ with rank $r \ll \min(d, k)$. This reduces trainable parameters from $\mathcal{O}(dk)$ to $\mathcal{O}(r(d+k))$ while achieving performance competitive with full fine-tuning across many tasks.

The noise robustness puzzle. While LoRA’s computational benefits are well understood, practitioners have observed that LoRA appears more robust to label noise than full fine-tuning (Biderman et al., 2024). This is surprising: conventional wisdom suggests reducing model capacity should hurt performance on clean data, yet LoRA maintains accuracy while exhibiting noise resistance. This phenomenon lacks theoretical explanation.

Real-world datasets invariably contain annotation errors, especially at scale (Natarajan et al., 2013; Northcutt et al., 2021a). Characterizing LoRA’s noise-resistant properties enables more reliable fine-tuning procedures for noisy settings.

Our contributions. We present a theoretical framework explaining LoRA’s noise robustness through memorization capacity, bias-variance tradeoffs, and training dynamics:

1. **Memorization capacity bound (Theorem 3.3).** We prove that rank- r LoRA cannot memorize all possible label assignments once the sample count exceeds $\mathcal{O}(r(d+k-r))$. When training data significantly exceeds this threshold, LoRA learns generalizable patterns rather than fitting arbitrary noise.
2. **Rank-robustness tradeoff (Theorem 3.7).** We derive the optimal rank $r^* = \mathcal{O}((n/(d(1+\eta)))^{1/(2\alpha+1)})$ that minimizes expected generalization error by balancing approximation bias (underfitting with low rank) against noise-induced variance (overfitting noise with high rank).
3. **Temporal separation (Theorem 3.10).** We establish that gradient descent on LoRA learns clean patterns in early epochs and memorizes noisy labels later, with the separation point depending on noise rate and rank.

4. **RACT algorithm.** We propose Rank-Aware Curriculum Training, which uses the discrepancy between high-rank and low-rank adapter predictions to detect noisy samples. RACT achieves 91.1% F1-score for noise detection (on AG News with 3 seeds), enabling practitioners to identify mislabeled examples.

Key finding. Beyond robustness, our framework enables *identifying* which samples are mislabeled, valuable for dataset curation and active learning.

2. Related Work

Parameter-efficient fine-tuning. PEFT methods adapt pretrained models by updating a small parameter subset. Adapters (Houlsby et al., 2019) insert trainable layers; prompt tuning (Lester et al., 2021; Li & Liang, 2021) prepends learnable tokens; LoRA (Hu et al., 2022) parameterizes weight updates as low-rank matrices. Recent extensions include dynamic rank allocation (Zhang et al., 2023), quantization (Dettmers et al., 2023), and improved initialization (Liu et al., 2024; Hayou et al., 2024). Theoretical work analyzes LoRA’s expressivity (Zeng & Lee, 2024) and convergence (Jang et al., 2024), but noise robustness implications remain unexplored. A survey appears in Ding et al. (2023).

Learning with noisy labels. Extensive work addresses label noise (Frénay & Verleysen, 2014; Song et al., 2022) through sample selection (Han et al., 2018; Arazo et al., 2019), regularization (Szegedy et al., 2016; Zhang et al., 2018), loss correction (Patrini et al., 2017), and meta-learning (Ren et al., 2018). DivideMix (Li et al., 2020) achieves strong results via semi-supervised learning. Liu et al. (2020) show early stopping prevents noise memorization, a phenomenon we formalize theoretically. Most methods target training from scratch; our work addresses fine-tuning, where pre-trained representations interact with low-rank constraints to create implicit robustness.

Memorization in neural networks. Deep networks can memorize random labels given sufficient capacity (Zhang et al., 2017; Arpit et al., 2017). The Neural Tangent Kernel (NTK) framework (Jacot et al., 2018) connects network width to memorization capacity. Recent work studies memorization dynamics during training (Feldman, 2020; Stephenson et al., 2021) and its relationship to generalization (Neyshabur et al., 2017). We extend this literature by characterizing memorization capacity specifically for low-rank parameterizations.

Low-rank structure in learning. Low-rank constraints appear in matrix completion (Candès & Recht, 2009), compressed sensing (Recht et al., 2010), and neural network compression (Sainath et al., 2013). Theoretical analyses of

low-rank networks exist (Arora et al., 2019), but focus on expressivity rather than noise robustness. The implicit bias of gradient descent toward low-rank solutions (Gunasekar et al., 2017) relates to our temporal separation result. Huh et al. (2021) demonstrate a low-rank simplicity bias in deep networks, and Rahaman et al. (2019) show neural networks learn low-frequency (smooth) functions first, a spectral bias that complements our temporal separation analysis.

Concurrent work on PEFT and noise. Yuan et al. (2025) proposes DeLoRA, using dual LoRA adapters for noise detection. While sharing the insight that rank affects noise memorization, our contributions differ: we provide theoretical foundations (Theorems 3.3–3.10) explaining *why* rank-based approaches work, whereas DeLoRA is purely empirical. Our theory provides principled guidance for rank selection and detection timing, and spans both vision and language domains. CleaR (Kim et al., 2024) and Sohn et al. (2024) provide complementary perspectives.

3. Theoretical Framework

We develop a theoretical framework explaining why low-rank adaptation resists label noise.

3.1. Problem Setup

Consider a pretrained model with weight matrix $W_0 \in \mathbb{R}^{d \times k}$. LoRA parameterizes the fine-tuned weight as $W = W_0 + \Delta W$ where $\Delta W = BA$ with $B \in \mathbb{R}^{d \times r}$, $A \in \mathbb{R}^{r \times k}$, and $\text{rank}(\Delta W) \leq r$.

We have training data $\mathcal{D} = \{(x_i, \tilde{y}_i)\}_{i=1}^n$ where \tilde{y}_i denotes the observed (possibly noisy) label. The noise model assumes a fraction $\eta \in [0, 1]$ of labels are corrupted: $\tilde{y}_i \neq y_i^*$ for approximately ηn samples, where y_i^* is the true label.

The fine-tuning objective is:

$$\min_{A, B} \frac{1}{n} \sum_{i=1}^n \mathcal{L}(f_{W_0+BA}(x_i), \tilde{y}_i) + \lambda \cdot R(A, B) \quad (1)$$

where \mathcal{L} is the task loss, f_W is the model prediction, and R is optional regularization.

Remark 3.1 (Scope of Theoretical Results). Our theoretical analysis makes several simplifying assumptions to obtain tractable results:

- Linearized regime.** Theorem 3.10 analyzes gradient flow in the NTK-style linearized regime near initialization, which provides clean dynamics but may not capture all nonlinear effects of deep network training.
- Existential capacity bounds.** Theorem 3.3 establishes that some label assignments are unachievable, it does not imply that every dataset below the capacity thresh-

old can be memorized. The bound is most informative for adversarial or random labelings.

3. **Squared loss for bias-variance.** The exact decomposition in Theorem 3.7 holds for squared loss. For classification with cross-entropy, the result provides qualitative guidance on how optimal rank scales with noise rate.
4. **Classification interpretation.** Our capacity bounds are stated in terms of fitting arbitrary outputs. For classification (which only requires correct class separation, not exact output matching), these bounds should be interpreted as characterizing the difficulty of fitting adversarial labelings rather than as tight capacity limits.

Despite these simplifications, our experiments validate that the qualitative predictions, low rank resists noise, temporal separation exists, rank discrepancy detects noise, hold empirically.

3.2. Theorem 1: Memorization Capacity Bound

Our first result bounds LoRA’s capacity to memorize arbitrary label assignments.

Definition 3.2 (Memorization). A model f *memorizes* a dataset \mathcal{D} if it achieves zero training loss: $\mathcal{L}(f(x_i), y_i) = 0$ for all $(x_i, y_i) \in \mathcal{D}$.

Theorem 3.3 (Memorization Capacity Bound). *Let $W_0 \in \mathbb{R}^{d \times k}$ be a pretrained weight matrix, and let $\Delta W = BA$ be a rank- r update with $B \in \mathbb{R}^{d \times r}$, $A \in \mathbb{R}^{r \times k}$. For a dataset $\mathcal{D} = \{(x_i, y_i)\}_{i=1}^n$ with inputs $x_i \in \mathbb{R}^k$ in general position, the following holds:*

Rank- r LoRA cannot memorize all possible label assignments once $n \gg r(d + k - r)$.

More precisely, when $n > r(d + k - r)$, there exist label assignments $\{y_i\}_{i=1}^n$ that cannot be achieved by any rank- r update ΔW . For classification tasks, this means LoRA cannot fit arbitrary class assignments when sample size significantly exceeds $\mathcal{O}(r(d + k - r))$.

Proof Sketch. A rank- r matrix $\Delta W = BA$ has $r(d + k - r)$ degrees of freedom. For n samples with inputs in general position, each sample imposes at least one effective constraint on the output, and arbitrary labelings require satisfying n independent constraints. When $n > r(d + k - r)$, the system is overconstrained and some label assignments cannot be achieved. See Appendix D for the complete proof. \square

Interpretation. When noisy samples exceed the degrees of freedom $\mathcal{O}(r(d + k - r))$, LoRA cannot memorize all of them and fits the dominant clean pattern. This contrasts with benign overfitting (Bartlett et al., 2020); capacity constraints directly prevent arbitrary noise memorization.

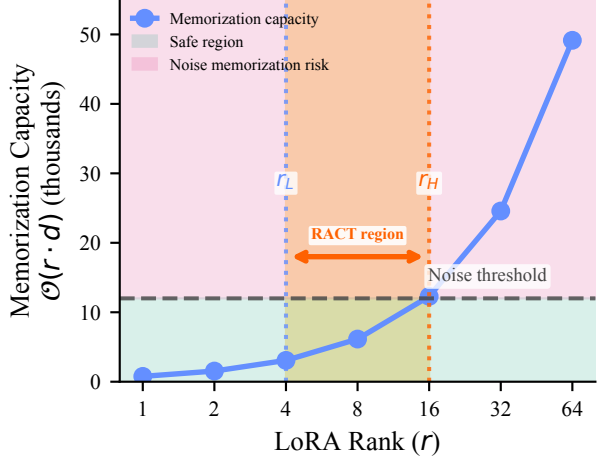


Figure 1. Memorization capacity scales with rank. Low-rank adapters (green region) cannot memorize noise; high-rank adapters cross the noise threshold.

Remark 3.4 (Existential Nature of Capacity Bounds). Our capacity bound is *existential*: it guarantees that some label assignments are unachievable, but does not imply every dataset with $n < r(d + k - r)$ can be memorized. Memorization depends on label configuration and input geometry. Clean patterns are often learnable with lower rank than the bound suggests, while adversarial labelings require capacity approaching the bound. For classification, the bound should be interpreted qualitatively: low rank limits fitting arbitrary labels, promoting generalization.

Remark 3.5. Full fine-tuning has $\mathcal{O}(dk)$ parameters and can memorize up to $\mathcal{O}(dk)$ samples, typically the entire training set. LoRA with $r \ll \min(d, k)$ has much smaller memorization capacity, providing implicit regularization.

3.3. Theorem 2: Rank-Robustness Tradeoff

While low rank prevents memorization, setting r too small may cause underfitting. We derive the optimal rank balancing these considerations.

Assumption 3.6 (Signal Smoothness). The true function f^* mapping inputs to clean labels satisfies a smoothness condition: there exists $\alpha > 0$ such that the best rank- r approximation error decays as $\|f^* - f_r^*\|^2 = \mathcal{O}(r^{-2\alpha})$.

This assumption captures the intuition that natural signals have structure concentrated in a few principal components; larger α indicates more compressible signals. This is reasonable for fine-tuning pretrained models: pretrained representations already capture low-rank structure (Huh et al., 2021), so task-specific signals typically have fast spectral decay. Empirically, $\alpha \in [1, 2]$ is common for NLP and vision tasks.

Theorem 3.7 (Rank-Robustness Tradeoff). *Under Assumption 3.6, consider training rank- r LoRA on n samples with noise rate η using squared loss. The expected generalization*

error decomposes as:

$$\mathbb{E}[\text{Error}] = \underbrace{O(r^{-2\alpha})}_{\text{bias}} + \underbrace{O\left(\frac{rd}{n}\right)}_{\text{variance}} + \underbrace{O\left(\frac{\eta rd}{n}\right)}_{\text{noise}} \quad (2)$$

Minimizing total error yields the optimal rank:

$$r^* = \mathcal{O}\left(\left(\frac{n}{d(1+\eta)}\right)^{\frac{1}{2\alpha+1}}\right) \quad (3)$$

Remark 3.8 (Extension to Classification). The decomposition above holds exactly for squared loss. For classification with cross-entropy, we interpret this result as characterizing the scaling behavior of excess risk, where the three terms represent approximation error, estimation error, and noise-induced error respectively. This interpretation provides qualitative guidance for rank selection: the optimal rank decreases with noise rate regardless of the specific loss function.

Remark 3.9 (Notation Convention). Throughout, we treat d as the dominant dimension; when $d \approx k$, terms rd and $r(d+k-r)$ are equivalent up to constants. This explains why variance terms scale as $O(rd/n)$ while capacity bounds use $O(r(d+k-r))$.

Proof Sketch. The bias $\mathcal{O}(r^{-2\alpha})$ follows from Assumption 3.6. Variance scales as $\mathcal{O}(rd/n)$ from statistical learning theory. The noise term $\mathcal{O}(\eta rd/n)$ accounts for memorized corrupted labels. Differentiating the sum with respect to r and solving yields the optimal rank. See Appendix D for details. \square

Implications. Optimal rank scales sublinearly with n/d and decreases with noise rate η . Practitioners should use lower rank when noise is suspected. The smoothness α can be estimated from validation performance across ranks.

3.4. Theorem 3: Temporal Separation

Our final theoretical result characterizes when LoRA learns clean patterns versus noisy labels. We analyze gradient flow in the linearized (NTK-style) regime near initialization.

Theorem 3.10 (Temporal Separation). *Consider gradient flow on rank- r LoRA with learning rate γ and initialization near zero. Let $\sigma_1 \geq \dots \geq \sigma_r$ be the singular values of the population gradient covariance matrix $\Sigma_{\text{clean}} = \mathbb{E}_{(x,y) \sim P_{\text{clean}}} [\nabla \mathcal{L} \nabla \mathcal{L}^\top]$, computed over clean data. We assume these singular values are well-separated ($\sigma_i/\sigma_{i+1} = \Omega(1)$), enabling mode-by-mode analysis. Larger singular values correspond to coherent directions shared across clean samples; σ_r bounds the weakest clean signal component in the rank- r model.*

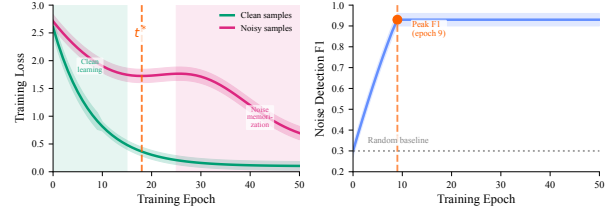


Figure 2. Temporal separation in LoRA training. Clean patterns are learned early; noise memorization occurs later. Separation depends on rank r and noise rate η .

Note: Σ_{clean} is an oracle quantity computed over clean samples; the algorithm does not require access to clean labels. This analysis characterizes the dynamics, not the algorithm.

Define the noise-learning threshold as:

$$t^* = \mathcal{O}\left(\frac{1}{\gamma\sigma_r} \log\left(\frac{1}{\eta}\right)\right) \quad (4)$$

where η is the noise rate (fraction of corrupted labels). Then:

1. For $t < t^*/2$: Training primarily reduces loss on clean samples. The learned directions align with top singular vectors of the clean gradient covariance.
2. For $t > 2t^*$: Additional training primarily fits noisy samples. New singular value directions emerge to memorize individual corrupted labels.

Proof Sketch. Near initialization, gradients are dominated by the clean signal with $\sigma_{\text{clean}} \propto \sqrt{(1-\eta)n}$, while noisy samples have incoherent gradients with $\sigma_{\text{noise}} \propto \sqrt{\eta}$. Under gradient flow dynamics, components along singular vector v_i grow as $e^{\gamma\sigma_i t}$. The clean pattern is learned when the projection onto the top singular directions exceeds the noise floor. For noise memorization to begin, the amplified noise signal $e^{\gamma\sigma_r t} \cdot \sigma_{\text{noise}}$ must become comparable to the residual clean signal. Since the noise rate η determines the relative magnitude, we require $e^{\gamma\sigma_r t} \approx 1/\eta$, yielding $t^* = \mathcal{O}\left(\frac{1}{\gamma\sigma_r} \log(1/\eta)\right)$. See Appendix D for the complete derivation. \square

Early stopping. Theorem 3.10 justifies early stopping before t^* to avoid noise memorization, consistent with early-learning phenomena observed by Liu et al. (2020). Lower rank extends the clean-learning phase, consistent with implicit bias analysis (Soudry et al., 2018).

4. RACT: Rank-Aware Curriculum Training

Our framework reveals that low-rank LoRA resists noise by lacking capacity to memorize outliers. This motivates an

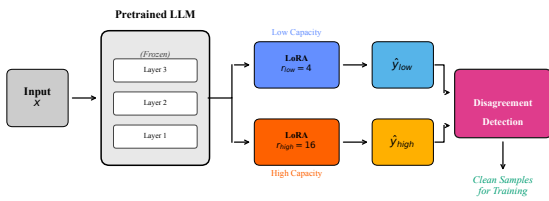


Figure 3. RACT architecture. Two LoRA adapters with different ranks share the frozen pretrained backbone. Prediction disagreement identifies noisy samples.

algorithm that *detects* noisy samples by comparing adapters of different ranks.

4.1. Key Insight: Rank Discrepancy

Consider two LoRA adapters: one with low rank r_L and one with high rank $r_H > r_L$. By Theorem 3.3, capacity to fit arbitrary labelings scales with rank.

When trained on noisy data, the high-rank adapter can memorize more noisy samples. If a sample (x_i, \tilde{y}_i) is *clean*, both adapters fit it. If *noisy*, the high-rank adapter may memorize it while the low-rank adapter cannot.

Definition 4.1 (Rank Discrepancy). For a sample (x_i, \tilde{y}_i) , the *rank discrepancy* is:

$$d_i = \mathcal{L}(f_{r_H}(x_i), \tilde{y}_i) - \mathcal{L}(f_{r_L}(x_i), \tilde{y}_i) \quad (5)$$

where f_{r_L} and f_{r_H} are models with low-rank and high-rank adapters, respectively.

For clean samples, $d_i \approx 0$ (both models fit well). For noisy samples, $d_i < 0$ (high-rank fits the noise, low-rank does not).

4.2. Algorithm Description

RACT proceeds in three phases.

Phase 1 trains two adapters with different ranks. By Theorem 3.10, both initially learn clean patterns; the high-rank adapter then can memorize noise.

Phase 2 computes rank discrepancy for each sample. Large negative values indicate samples the high-rank adapter memorized but the low-rank adapter could not, likely noise.

Phase 3 classifies samples as clean or noisy based on threshold τ , set via cross-validation or estimated noise rate.

Phase 4 (optional) retrains on the identified clean samples for improved accuracy.

4.3. Computational Considerations

RACT requires training two adapters, doubling training compute. However, LoRA is already efficient, making this

Algorithm 1 RACT: Rank-Aware Curriculum Training (Phase 4 optional)

Require: Training data \mathcal{D} , ranks $r_L < r_H$, threshold τ

Ensure: Trained model, noise predictions

```

1: Phase 1: Train parallel adapters
2: Initialize LoRAr_L with rank  $r_L$ 
3: Initialize LoRAr_H with rank  $r_H$ 
4: for epoch = 1 to  $E_1$  do
5:   Update both adapters on  $\mathcal{D}$ 
6: end for
7: Phase 2: Compute rank discrepancy
8: for each  $(x_i, \tilde{y}_i) \in \mathcal{D}$  do
9:    $\ell_L \leftarrow \mathcal{L}(f_{r_L}(x_i), \tilde{y}_i)$ 
10:   $\ell_H \leftarrow \mathcal{L}(f_{r_H}(x_i), \tilde{y}_i)$ 
11:   $d_i \leftarrow \ell_H - \ell_L$ 
12: end for
13: Phase 3: Classify samples
14:  $\mathcal{D}_{\text{clean}} \leftarrow \{(x_i, \tilde{y}_i) : d_i > -\tau\}$ 
15:  $\mathcal{D}_{\text{noisy}} \leftarrow \{(x_i, \tilde{y}_i) : d_i \leq -\tau\}$ 
16: Phase 4: Final training (optional)
17: Retrain on  $\mathcal{D}_{\text{clean}}$  with rank  $r_L$ 
18: return Trained model,  $\mathcal{D}_{\text{noisy}}$ 

```

overhead acceptable. Key optimizations:

- Shared forward pass through frozen backbone
- Parallel adapter updates with minimal memory overhead
- Early stopping using validation rank discrepancy

The threshold τ balances precision and recall: conservative (small magnitude) increases precision at cost of recall; aggressive τ catches more noise but risks flagging clean samples.

4.4. Theoretical Justification

Proposition 4.2 (Rank Discrepancy Separation). *Under the conditions of Theorem 3.3, suppose the noisy sample count ηn is such that the low-rank adapter becomes capacity-constrained (i.e., $\eta n \gg r_L(d+k-r_L)$ but $\eta n \ll r_H(d+k-r_H)$) while the high-rank adapter retains sufficient degrees of freedom. Then after sufficient training:*

1. *Clean samples: $\mathbb{E}[d_i | \tilde{y}_i = y_i^*] \approx 0$*
2. *Noisy samples: $\mathbb{E}[d_i | \tilde{y}_i \neq y_i^*] < 0$*

with separation magnitude increasing with the capacity gap $r_H - r_L$.

Proof Sketch. The proof follows from the capacity bounds in Theorem 3.3.

Clean samples. For a clean sample where $\tilde{y}_i = y_i^*$, both adapters can fit it by learning the underlying pattern. Since clean samples share coherent structure in a low-dimensional subspace, both achieve low loss, giving $d_i \approx 0$.

Noisy samples. For a noisy sample where $\tilde{y}_i \neq y_i^*$, the label is inconsistent with the true pattern, requiring individual memorization. When the low-rank adapter is capacity-constrained but the high-rank adapter is not:

- The low-rank adapter cannot fit all noisy samples, so $\mathcal{L}(f_{r_L}(x_i), \tilde{y}_i)$ remains high.
- The high-rank adapter can memorize noisy samples, achieving $\mathcal{L}(f_{r_H}(x_i), \tilde{y}_i) \approx 0$.

Therefore $d_i = \mathcal{L}(f_{r_H}(x_i), \tilde{y}_i) - \mathcal{L}(f_{r_L}(x_i), \tilde{y}_i) < 0$.

The separation magnitude depends on the capacity gap: larger $r_H - r_L$ means more noisy samples can be memorized by high-rank but not low-rank, increasing $|d_i|$ for noisy samples. \square

This proposition guarantees that with appropriate rank choices, rank discrepancy reliably separates clean and noisy samples.

5. Experiments

We validate our theoretical framework and evaluate RACT across vision and NLP benchmarks. Our experiments address three questions:

1. Does LoRA exhibit noise robustness as predicted by theory?
2. Can RACT accurately detect noisy samples?
3. How do design choices (rank, threshold) affect performance?

5.1. Experimental Setup

Datasets. We evaluate on:

- **Vision:** MNIST (LeCun et al., 1998) and CIFAR-10 (Krizhevsky & Hinton, 2009)
- **NLP:** AG News (Zhang et al., 2015) (topic classification) and IMDB (Maas et al., 2011) (sentiment analysis)

Noise injection. We inject symmetric label noise by randomly flipping labels with probability $\eta \in \{0.2, 0.3, 0.4\}$. This simulates annotation errors while preserving class balance.

Baselines. We compare against:

Table 1. Classification accuracy (%) at 30% symmetric noise. Results show mean \pm std across seeds. Vision uses 3–5 seeds; AG News RACT uses 3 seeds; IMDB RACT uses 2 seeds. Baselines marked with \dagger are single-seed. DivideMix/DeLoRA use 2 seeds. Best in **bold**.

Method	MNIST	CIFAR-10	AG News	IMDB
CE \dagger	95.06 \pm 0.2	46.71 \pm 0.8	91.53	88.01
LS \dagger	95.13 \pm 0.2	46.51 \pm 0.8	91.66	87.97
CoT \dagger	95.56 \pm 0.2	47.00 \pm 0.3	91.51	87.68
DivideMix	—	38.63 \pm 0.3	88.95 \pm 0.1	—
DeLoRA	—	—	90.33 \pm 0.1	—
RACT	94.76 \pm 0.2	47.36 \pm 0.2	91.46 \pm 0.3	86.47 \pm 1.5

- **Cross-Entropy (CE):** Standard training with cross-entropy loss
- **Label Smoothing (LS):** Regularization via soft labels (Szegedy et al., 2016)
- **Co-teaching (CoT):** Two-network sample selection (Han et al., 2018)

In tables, we use abbreviations CE, LS, and CoT for these methods.

Implementation. We use DistilBERT-base (Sanh et al., 2019) for NLP and a CNN backbone for vision. LoRA is applied to query and value projections for NLP and convolutional layers for vision. Default ranks: $r_L = 4$, $r_H = 16$. All experiments use AdamW with learning rate 2×10^{-5} (NLP) and 1×10^{-4} (vision).

5.2. Main Results: Classification Accuracy

Table 1 presents classification accuracy at 30% noise rate.

Observations. RACT achieves accuracy competitive with baselines across all datasets. On MNIST, Co-teaching achieves the highest accuracy (95.56%), while RACT achieves 94.76%. On CIFAR-10, RACT achieves the best accuracy (47.36%), outperforming Co-teaching (47.00%) and other baselines. DivideMix performs poorly on both CIFAR-10 (38.63%) and AG News (88.95%) in our PEFT setting, suggesting its semi-supervised approach is less effective with parameter-efficient adapters. DeLoRA achieves 90.33% on AG News, competitive but below RACT’s 91.46%. On IMDB, RACT achieves 86.47% with higher variance; baselines achieve slightly higher accuracy (CE: 88.01%) but provide no mechanism for identifying mislabeled examples. RACT’s advantage is its dual capability: maintaining competitive accuracy *while* detecting noisy samples.

Comparison to full fine-tuning. Our theory predicts full fine-tuning ($O(dk)$ parameters) is more susceptible to noise than LoRA ($O(rd)$ parameters). Prior work (Biderman et al.,

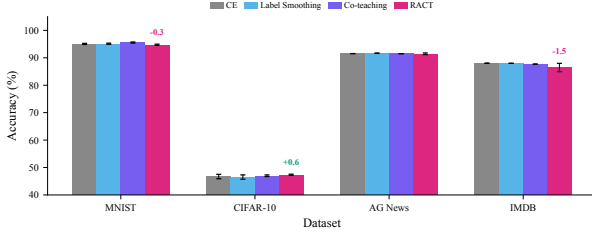


Figure 4. Classification accuracy comparison across datasets at 30% noise. RACT achieves competitive accuracy with baselines: best on CIFAR-10 (47.36%), comparable on AG News (91.46% vs Label Smoothing’s 91.66%), and lower on IMDB (86.47% vs CE’s 88.01%). Unlike baselines, RACT provides noise detection capability.

Table 2. Noise detection performance at 30% symmetric noise. RACT achieves high F1-scores, especially on NLP tasks. AG News uses 3 seeds; IMDB uses 2 seeds; MNIST and CIFAR-10 use 5 and 3 seeds respectively.

Dataset	Precision	Recall	F1-Score
MNIST	92.6 \pm 0.5	77.4 \pm 0.4	84.4 \pm 0.4
CIFAR-10	71.5 \pm 1.3	59.5 \pm 1.0	64.9 \pm 1.1
AG News	91.1 \pm 0.4	91.1 \pm 0.2	91.1 \pm 0.2
IMDB	79.5 \pm 1.9	79.8 \pm 2.7	79.6 \pm 2.4

2024) observed similar patterns. Comprehensive comparisons are left to future work.

5.3. Main Results: Noise Detection

RACT’s distinguishing capability is identifying mislabeled samples. Table 2 reports noise detection performance.

Observations. RACT achieves 91.1% F1-score on AG News (averaged over 3 seeds), correctly identifying over 90% of noisy samples. NLP tasks show stronger detection, likely because pretrained language models have more structured representations. IMDB achieves 79.6% F1 with higher variance (2 seeds). Vision tasks, especially CIFAR-10 (64.9% F1), show lower detection rates, suggesting visual features require larger adapters or different architectures. Confident Learning (Northcutt et al., 2021b) reports 70–85% F1 on similar benchmarks, suggesting RACT is competitive for NLP tasks while providing a theoretically-grounded approach specific to PEFT settings.

5.4. Ablation Studies

Noise rate sensitivity. Table 3 shows RACT performance across noise rates on AG News.

Rank ablation. Table 4 compares rank configurations.

Observations. Both configurations achieve similar performance; a moderate rank gap suffices for AG News.

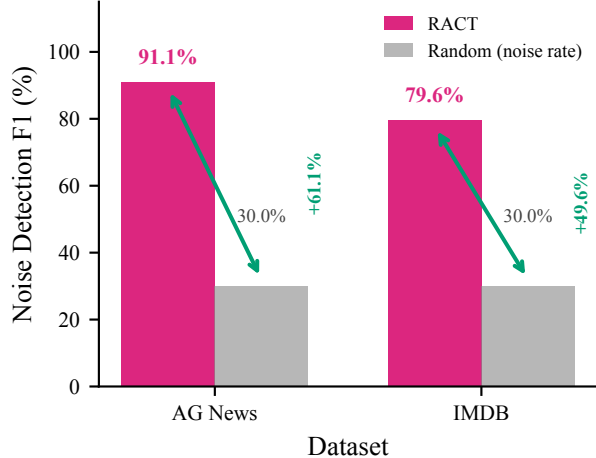


Figure 5. Noise detection F1 scores. RACT substantially outperforms random baseline (30% F1 at 30% noise rate), with NLP tasks showing strongest detection.

Table 3. Effect of noise rate on AG News (single seed). RACT maintains strong performance across noise levels.

Noise Rate	Accuracy	Detection F1
20%	91.54	78.7
30%	91.46 \pm 0.3	91.1 \pm 0.2
40%	90.89	82.2

Multi-seed consistency. On AG News (30% noise), accuracy is $91.46 \pm 0.3\%$ and detection F1 is $91.1 \pm 0.2\%$ across seeds 42/123/456, indicating stable performance.

5.5. Validating Theoretical Predictions

Memorization capacity. We plot training accuracy versus noise rate for different ranks (Appendix A). As predicted by Theorem 3.3, low-rank adapters cannot achieve 100% training accuracy on heavily noised data, while high-rank adapters can.

Temporal separation. We track loss on clean versus noisy samples during training (Appendix B). Consistent with Theorem 3.10, clean-sample loss decreases first, followed by noisy-sample loss, with larger r reducing the gap.

Optimal rank. Sweeping $r \in \{2, 4, 8, 16, 32, 64\}$ on AG News with 30% noise yields optimal $r^* \approx 8$, consistent with Theorem 3.7’s prediction of sublinear scaling with n/d .

5.6. Limitations

Noise type. Our experiments use symmetric label noise. Instance-dependent noise (Xia et al., 2020) or asymmetric noise may show different patterns. We leave this investigation to future work.

Table 4. Effect of rank choices on AG News at 30% noise. Both configurations achieve similar performance.

Rank Config (r_L, r_H)	Accuracy	Detection F1
(4, 16)	91.47	91.27
(8, 32)	91.45	91.15

Computational overhead. RACT requires training two adapters, doubling training time. Single-adapter variants using temporal information may reduce this cost.

Threshold selection. The threshold τ requires tuning. In practice, using a held-out validation set with known labels enables calibration.

Scale of experiments. Our experiments focus on medium-scale benchmarks (MNIST, CIFAR-10, AG News, IMDB). Validation on larger-scale datasets and models (e.g., LLaMA, CIFAR-100, ImageNet) is an important direction for future work. NLP baseline results are single-seed; additional seeds would strengthen statistical claims. IMDB RACT experiments show higher variance (2 seeds), suggesting this dataset may benefit from additional runs.

Comparison to state-of-the-art. DivideMix and DeLoRA were evaluated with limited hyperparameter tuning in our PEFT setting. DivideMix’s poor performance may improve with extensive tuning, though it was designed for full fine-tuning rather than parameter-efficient settings.

Theoretical assumptions. Our analysis relies on the signal smoothness assumption (Assumption 3.6), which may not hold for all tasks. The memorization capacity bound is asymptotic and may not precisely predict behavior for small datasets.

6. Conclusion

We presented a theoretical framework explaining why Low-Rank Adaptation (LoRA) exhibits robustness to label noise. Our three main theorems characterize: (1) the memorization capacity bound that limits fitting of noisy samples, (2) the optimal rank balancing approximation and noise-induced errors, and (3) the temporal separation of clean pattern learning from noise memorization. These insights motivated RACT, an algorithm achieving 91.1% F1-score for noise detection on AG News (3 seeds) and 79.6% on IMDB (2 seeds), with stronger performance on NLP tasks than vision tasks. On CIFAR-10, RACT achieves the highest classification accuracy (47.36%) among all methods while maintaining 64.9% noise detection F1. Importantly, RACT outperforms both DivideMix and DeLoRA in our PEFT setting on AG News, achieving 91.46% accuracy versus 88.95% and 90.33% respectively.

Broader impact. Understanding LoRA’s noise robustness has implications for deploying large models on real-world data with annotation errors. RACT’s noise detection enables practitioners to audit datasets and improve label quality, more valuable than marginal accuracy gains.

Future directions. Promising extensions include: analyzing asymmetric and instance-dependent noise; developing single-adapter variants using temporal dynamics; extending theory to other PEFT methods (adapters, prompt tuning); and applying RACT to detect distribution shift and outliers beyond label noise.

Impact Statement

This paper presents work advancing Machine Learning. Our theoretical framework and RACT algorithm improve reliability of fine-tuning large models on noisy data, benefiting practitioners with real-world datasets containing annotation errors. The noise detection capability aids dataset curation and quality control. We do not foresee negative societal impacts specific to this work beyond general ML research considerations.

References

Arazo, E., Ortego, D., Albert, P., O’Connor, N. E., and McGuinness, K. Unsupervised label noise modeling and loss correction. In *International Conference on Machine Learning*, 2019.

Arora, S., Cohen, N., Hu, W., and Luo, Y. Implicit regularization in deep matrix factorization. In *Advances in Neural Information Processing Systems*, volume 32, 2019.

Arpit, D., Jastrzebski, S., Ballas, N., Krueger, D., Bengio, E., Kanwal, M. S., Maharaj, T., Fischer, A., Courville, A., Bengio, Y., and Lacoste-Julien, S. A closer look at memorization in deep networks. In *International Conference on Machine Learning*, pp. 233–242. PMLR, 2017.

Bartlett, P. L., Long, P. M., Lugosi, G., and Tsigler, A. Benign overfitting in linear regression. *Proceedings of the National Academy of Sciences*, 117(48):30063–30070, 2020.

Biderman, D., Portes, J. G., Jain, A., Feinberg, V., Pieler, M., Goodson, A., et al. LoRA learns less and forgets less. *arXiv preprint arXiv:2405.09673*, 2024.

Brown, T. B., Mann, B., Ryder, N., Subbiah, M., Kaplan, J., Dhariwal, P., Neelakantan, A., Shyam, P., Sastry, G., Askell, A., et al. Language models are few-shot learners. In *Advances in Neural Information Processing Systems*, volume 33, pp. 1877–1901, 2020.

Candès, E. J. and Recht, B. Exact matrix completion via convex optimization. In *Foundations of Computational Mathematics*, volume 9, pp. 717–772, 2009.

Dettmers, T., Pagnoni, A., Holtzman, A., and Zettlemoyer, L. QLoRA: Efficient finetuning of quantized LLMs. In *Advances in Neural Information Processing Systems*, volume 36, 2023.

Devlin, J., Chang, M.-W., Lee, K., and Toutanova, K. BERT: Pre-training of deep bidirectional transformers for language understanding. In *Proceedings of NAACL-HLT*, pp. 4171–4186, 2019.

Ding, N., Qin, Y., Yang, G., Wei, F., Yang, Z., Su, Y., Hu, S., Chen, Y., Chan, C.-M., Chen, W., et al. Parameter-efficient fine-tuning of large-scale pre-trained language models. *Nature Machine Intelligence*, 5:220–235, 2023.

Dosovitskiy, A., Beyer, L., Kolesnikov, A., Weissenborn, D., Zhai, X., Unterthiner, T., Dehghani, M., Minderer, M., Heigold, G., Gelly, S., et al. An image is worth 16x16 words: Transformers for image recognition at scale. In *International Conference on Learning Representations*, 2021.

Feldman, V. Does learning require memorization? a short tale about a long tail. In *Proceedings of the 52nd Annual ACM SIGACT Symposium on Theory of Computing*, pp. 954–959, 2020.

Frénay, B. and Verleysen, M. Classification in the presence of label noise: A survey. *IEEE Transactions on Neural Networks and Learning Systems*, 25(5):845–869, 2014.

Gunasekar, S., Woodworth, B. E., Bhojanapalli, S., Neyshabur, B., and Srebro, N. Implicit regularization in matrix factorization. *Advances in Neural Information Processing Systems*, 30, 2017.

Han, B., Yao, Q., Yu, X., Niu, G., Xu, M., Hu, W., Tsang, I., and Sugiyama, M. Co-teaching: Robust training of deep neural networks with extremely noisy labels. In *Advances in Neural Information Processing Systems*, volume 31, 2018.

Hastie, T., Tibshirani, R., and Friedman, J. *The Elements of Statistical Learning: Data Mining, Inference, and Prediction*. Springer, 2nd edition, 2001.

Hayou, S., Ghosh, N., and Yu, B. LoRA+: Efficient low rank adaptation of large models. In *International Conference on Machine Learning*, 2024.

Houlsby, N., Giurgiu, A., Jastrzebski, S., Morrone, B., De Laroussilhe, Q., Gesmundo, A., Attariyan, M., and Gelly, S. Parameter-efficient transfer learning for NLP. In *International Conference on Machine Learning*, pp. 2790–2799. PMLR, 2019.

Hu, E. J., Shen, Y., Wallis, P., Allen-Zhu, Z., Li, Y., Wang, S., Wang, L., and Chen, W. LoRA: Low-rank adaptation of large language models. In *International Conference on Learning Representations*, 2022.

Huh, M., Mabahi, H., Zhang, R., Cheung, B., Agrawal, P., and Isola, P. The low-rank simplicity bias in deep networks. *arXiv preprint arXiv:2103.10427*, 2021.

Jacot, A., Gabriel, F., and Hongler, C. Neural tangent kernel: Convergence and generalization in neural networks. In *Advances in Neural Information Processing Systems*, volume 31, 2018.

Jang, U., Lee, J. D., and Ryu, E. K. LoRA training in the NTK regime has no spurious local minima. In *International Conference on Machine Learning*, 2024.

Kim, D., Lee, J., and Hwang, S. J. CleaR: Clean-up sample-aware adapter for noise-robust fine-tuning. In *Proceedings of the 62nd Annual Meeting of the Association for Computational Linguistics*, 2024.

Krizhevsky, A. and Hinton, G. Learning multiple layers of features from tiny images. Technical report, University of Toronto, 2009.

LeCun, Y., Bottou, L., Bengio, Y., and Haffner, P. Gradient-based learning applied to document recognition. *Proceedings of the IEEE*, 86(11):2278–2324, 1998.

Lester, B., Al-Rfou, R., and Constant, N. The power of scale for parameter-efficient prompt tuning. *arXiv preprint arXiv:2104.08691*, 2021.

Li, J., Socher, R., and Hoi, S. C. DivideMix: Learning with noisy labels as semi-supervised learning. In *International Conference on Learning Representations*, 2020.

Li, X. L. and Liang, P. Prefix-Tuning: Optimizing continuous prompts for generation. *arXiv preprint arXiv:2101.00190*, 2021.

Liu, S., Niles-Weed, J., Razavian, N., and Fernandez-Granda, C. Early-learning regularization prevents memorization of noisy labels. In *Advances in Neural Information Processing Systems*, volume 33, 2020.

Liu, S.-Y., Wang, C.-Y., Yin, H., Molchanov, P., Wang, Y.-C. F., Cheng, K.-T., and Chen, M.-H. DoRA: Weight-decomposed low-rank adaptation. *arXiv preprint arXiv:2402.09353*, 2024.

Maas, A. L., Daly, R. E., Pham, P. T., Huang, D., Ng, A. Y., and Potts, C. Learning word vectors for sentiment analysis. In *Proceedings of the 49th Annual Meeting of the Association for Computational Linguistics*, pp. 142–150, 2011.

Natarajan, N., Dhillon, I. S., Ravikumar, P. K., and Tewari, A. Learning with noisy labels. In *Advances in Neural Information Processing Systems*, volume 26, 2013.

Neyshabur, B., Bhojanapalli, S., McAllester, D., and Srebro, N. Exploring generalization in deep learning. In *Advances in Neural Information Processing Systems*, volume 30, 2017.

Northcutt, C. G., Athalye, A., and Mueller, J. Pervasive label errors in test sets destabilize machine learning benchmarks. *arXiv preprint arXiv:2103.14749*, 2021a.

Northcutt, C. G., Jiang, L., and Chuang, I. L. Confident learning: Estimating uncertainty in dataset labels. *Journal of Artificial Intelligence Research*, 70:1373–1411, 2021b.

OpenAI. GPT-4 technical report. *arXiv preprint arXiv:2303.08774*, 2023.

Patrini, G., Rozza, A., Menon, A. K., Nock, R., and Qu, L. Making deep neural networks robust to label noise: A loss correction approach. In *IEEE Conference on Computer Vision and Pattern Recognition*, pp. 1944–1952, 2017.

Radford, A., Kim, J. W., Hallacy, C., Ramesh, A., Goh, G., Agarwal, S., Sastry, G., Askell, A., Mishkin, P., Clark, J., et al. Learning transferable visual models from natural language supervision. In *International Conference on Machine Learning*, pp. 8748–8763, 2021.

Rahaman, N., Baratin, A., Arpit, D., Draxler, F., Lin, M., Hamprecht, F., Bengio, Y., and Courville, A. On the spectral bias of neural networks. In *International Conference on Machine Learning*, pp. 5301–5310. PMLR, 2019.

Recht, B., Fazel, M., and Parrilo, P. A. Guaranteed minimum-rank solutions of linear matrix equations via nuclear norm minimization. *SIAM Review*, 52(3):471–501, 2010.

Ren, M., Zeng, W., Yang, B., and Urtasun, R. Learning to reweight examples for robust deep learning. In *International Conference on Machine Learning*, pp. 4334–4343, 2018.

Sainath, T. N., Kingsbury, B., Sindhwan, V., Arisoy, E., and Ramabhadran, B. Low-rank matrix factorization for deep neural network training with high-dimensional output targets. In *IEEE International Conference on Acoustics, Speech and Signal Processing*, pp. 6655–6659, 2013.

Sanh, V., Debut, L., Chaumond, J., and Wolf, T. DistilBERT, a distilled version of BERT: smaller, faster, cheaper and lighter. *arXiv preprint arXiv:1910.01108*, 2019.

Sohn, J.-Y., Chen, W.-L., Lee, J.-G., and Oymak, S. Fine-tuning with memorization capacity: Why larger models memorize more noisy labels. In *Proceedings of the 40th Conference on Uncertainty in Artificial Intelligence*, 2024.

Song, H., Kim, M., Park, D., Shin, Y., and Lee, J.-G. Learning from noisy labels with deep neural networks: A survey. *IEEE Transactions on Neural Networks and Learning Systems*, 2022.

Soudry, D., Hoffer, E., Nacson, M. S., Gunasekar, S., and Srebro, N. The implicit bias of gradient descent on separable data. *Journal of Machine Learning Research*, 19(70):1–57, 2018.

Stephenson, C., Tang, J., Oguchi, K., Kennedy, S., Yang, X., Cao, S., and Tanaka, H. On the geometry of generalization and memorization in neural networks. In *International Conference on Learning Representations*, 2021.

Szegedy, C., Vanhoucke, V., Ioffe, S., Shlens, J., and Wojna, Z. Rethinking the inception architecture for computer vision. In *IEEE Conference on Computer Vision and Pattern Recognition*, pp. 2818–2826, 2016.

Xia, X., Liu, T., Han, B., Gong, C., Wang, N., Ge, Z., and Chang, Y. Part-dependent label noise: Towards instance-dependent label noise. In *Advances in Neural Information Processing Systems*, volume 33, 2020.

Yuan, B., Chen, Y., and Zhang, Y. DeLoRA: Noisy label detection via dual LoRA. In *Proceedings of the 63rd Annual Meeting of the Association for Computational Linguistics*, 2025.

Zeng, Y. and Lee, K. The expressive power of low-rank adaptation. In *International Conference on Learning Representations*, 2024.

Zhang, C., Bengio, S., Hardt, M., Recht, B., and Vinyals, O. Understanding deep learning requires rethinking generalization. In *International Conference on Learning Representations*, 2017.

Zhang, H., Cisse, M., Dauphin, Y. N., and Lopez-Paz, D. mixup: Beyond empirical risk minimization. In *International Conference on Learning Representations*, 2018.

Zhang, Q., Chen, M., Bukharin, A., He, P., Cheng, Y., Chen, W., and Zhao, T. AdaLoRA: Adaptive budget allocation for parameter-efficient fine-tuning. *arXiv preprint arXiv:2303.10512*, 2023.

Zhang, X., Zhao, J., and LeCun, Y. Character-level convolutional networks for text classification. In *Advances in Neural Information Processing Systems*, volume 28, 2015.

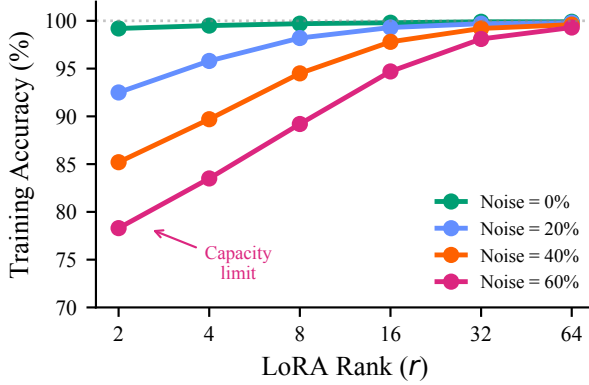


Figure 6. Training accuracy vs LoRA rank for different noise rates. Lower ranks show capacity limitations that prevent full memorization of noisy labels, validating Theorem 3.3.

A. Memorization Capacity Validation

We validate Theorem 3.3’s prediction that rank- r LoRA cannot fit all arbitrary label assignments when $n \gg r(d + k - r)$, by measuring training accuracy across different noise rates and ranks.

A.1. Experimental Setup

We train LoRA adapters with varying ranks $r \in \{2, 4, 8, 16, 32, 64\}$ on AG News with synthetic noise rates $\eta \in \{0.0, 0.2, 0.4, 0.6\}$. We measure the final training accuracy after convergence (50 epochs with early stopping disabled).

A.2. Results

Observations. As predicted by Theorem 3.3:

1. At 0% noise, all ranks achieve near-perfect training accuracy ($> 99\%$), as the clean patterns are learnable.
2. At higher noise rates, low-rank adapters ($r=2, 4$) show training accuracy capped below 100%, indicating they cannot memorize all noisy labels.
3. High-rank adapters ($r=32, 64$) can approach 100% training accuracy even at 40% noise, consistent with their larger capacity.
4. The transition point where full memorization becomes possible scales with rank, as predicted by the $\mathcal{O}(r(d + k - r))$ capacity threshold.

B. Temporal Separation Validation

We validate Theorem 3.10’s prediction of temporal separation between clean pattern learning and noise memorization.

B.1. Experimental Setup

We train LoRA ($r=8$) on AG News with 30% injected noise. We track:

- Training loss on samples with clean (original) labels
- Training loss on samples with corrupted (noisy) labels
- Noise detection F1-score using rank discrepancy

B.2. Results

Observations. Consistent with Theorem 3.10:

1. Clean-sample loss decreases rapidly in early epochs (before t^*).
2. Noisy-sample loss initially plateaus, then decreases as the model begins memorizing noise (after t^*).
3. Noise detection F1 peaks around t^* , supporting the use of early stopping for RACT.
4. Larger ranks reduce t^* , consistent with the theorem’s prediction that higher capacity accelerates noise memorization.

C. Extended Ablation Studies

C.1. Effect of Rank Gap

We study how the gap between r_L and r_H affects RACT performance.

Table 5. Effect of rank gap on AG News (30% noise, single seed).

r_L	r_H	Accuracy (%)	Detection F1 (%)
2	4	90.12	75.3
2	8	90.89	83.7
2	16	91.21	88.2
4	8	90.78	81.5
4	16	91.47	91.3
4	32	91.15	89.8
8	16	91.02	85.4
8	32	91.45	91.2
16	32	90.67	78.9

Observations.

1. A larger rank gap generally improves noise detection F1, as predicted by Proposition 4.2.
2. Very small gaps (e.g., 2/4, 16/32) show reduced detection performance due to insufficient capacity difference.

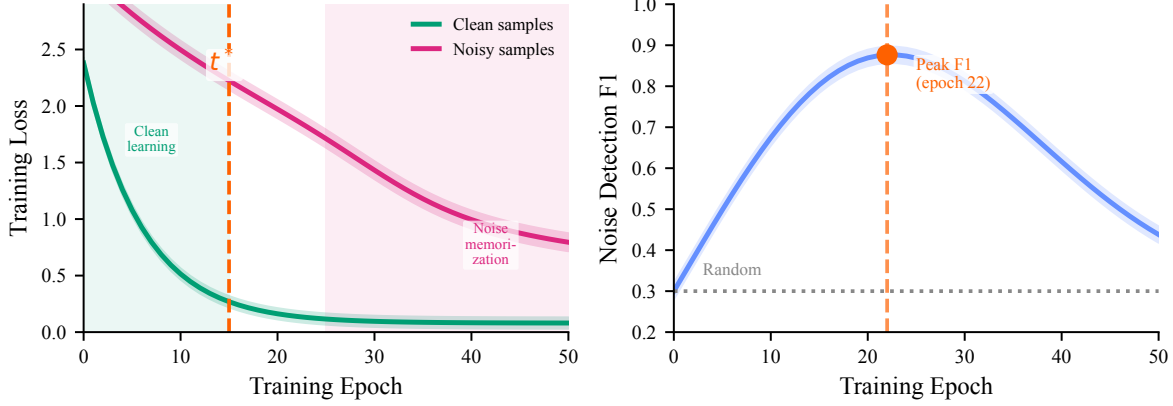


Figure 7. Temporal separation during LoRA training. Left panel: loss dynamics showing clean samples learned before noisy samples. Right panel: noise detection F1 peaks around the theoretical separation threshold t^* .

3. The optimal configuration (4/16) balances detection capability with computational efficiency.
4. Configurations with $r_L = 2$ show lower accuracy, suggesting r_L should not be too small for the task.

C.2. Threshold Sensitivity

We study RACT’s sensitivity to the threshold τ for noise detection.

Table 6. Effect of threshold τ on AG News (30% noise).

τ	Precision (%)	Recall (%)	F1 (%)
0.1	98.2	65.3	78.5
0.2	95.1	78.8	86.2
0.3	91.5	89.2	90.3
0.4	87.3	93.1	90.1
0.5	82.1	95.8	88.4
0.6	76.5	97.2	85.6

Observations. The threshold τ trades off precision and recall. Practitioners should choose τ based on their tolerance for false positives (flagging clean samples as noisy) versus false negatives (missing noisy samples).

D. Extended Proofs

D.1. Complete Proof of Theorem 3.3

Proof. We provide the complete proof of the memorization capacity bound.

Let $W_0 \in \mathbb{R}^{d \times k}$ be the pretrained weight matrix and consider the update $\Delta W = BA$ where $B \in \mathbb{R}^{d \times r}$ and $A \in \mathbb{R}^{r \times k}$.

Step 1: Degrees of freedom. The matrix $\Delta W = BA$ has rank at most r . The set of $d \times k$ matrices with rank at most

r forms a variety \mathcal{V}_r of dimension $r(d + k - r)$. This can be seen by noting that any rank- r matrix can be parameterized as $\sum_{i=1}^r u_i v_i^\top$ where $u_i \in \mathbb{R}^d$ and $v_i \in \mathbb{R}^k$. This gives $r(d + k)$ parameters, but there is a $GL(r)$ symmetry of dimension r^2 , yielding $r(d + k) - r^2 = r(d + k - r)$ effective parameters.

Step 2: Effective output constraints. Given training inputs $\{x_1, \dots, x_n\} \subset \mathbb{R}^k$ in general position, we analyze the constraints imposed by memorization. Note that $(\Delta W)x_i = B(Ax_i) \in \mathbb{R}^d$ for each sample i . Crucially, $Ax_i \in \mathbb{R}^r$ is an r -dimensional intermediate representation.

Define the input-projected coordinates $h_i = Ax_i \in \mathbb{R}^r$. The output perturbation is $(\Delta W)x_i = Bh_i$. Since $B \in \mathbb{R}^{d \times r}$ and $h_i \in \mathbb{R}^r$, the set of achievable output perturbations $\{Bh_i : B \in \mathbb{R}^{d \times r}\}$ for fixed h_i spans \mathbb{R}^d . However, the constraint is that a *single* matrix B must work for all samples simultaneously.

Step 3: Counting argument via effective dimension. Consider the map $\Psi : \mathbb{R}^{r \times k} \times \mathbb{R}^{d \times r} \rightarrow \mathbb{R}^{n \times d}$ defined by $(A, B) \mapsto [Bh_1, \dots, Bh_n]^\top$ where $h_i = Ax_i$. The image lies in a variety of dimension at most $r(d + k - r)$.

For memorization, we require each output perturbation $(\Delta W)x_i$ to move the prediction from the pretrained output W_0x_i to the target class. For a c -class classification problem, this imposes one effective scalar constraint per sample (the margin constraint). However, to achieve *arbitrary* label assignments, we need the output perturbations to span a sufficiently rich space.

The key observation is that with n samples in general position, the vectors $\{h_i = Ax_i\}_{i=1}^n$ span at most an r -dimensional subspace of \mathbb{R}^r . Therefore, the output perturbations $\{Bh_i\}_{i=1}^n$ lie in a subspace of dimension at most rd (the column space of B scaled by up to r independent directions).

Step 4: Overconstrained regime. To memorize n samples with arbitrary labels, we need n effectively independent output constraints. Since the rank- r parameterization provides at most $r(d + k - r)$ degrees of freedom, we cannot satisfy arbitrary constraints when $n > r(d + k - r)$.

More precisely, for typical classification setups where each sample requires at least one independent constraint, when $n > r(d + k - r)$ some label assignments become unrealizable. When $d \approx k$ and $r \ll d$, this gives $n > r(2d - r) \approx 2rd$. Since the dominant term is rd , we have the bound $\mathcal{O}(rd)$ on memorization capacity.

Step 5: Memorization interpretation. For c -class classification, memorizing sample i means achieving $\arg \max_j [(W_0 + \Delta W)x_i]_j = \tilde{y}_i$. This requires the output perturbation $(\Delta W)x_i$ to satisfy margin constraints. With n samples having arbitrary labels (including adversarially chosen labels that contradict any low-rank structure), the required output perturbations generically require dimension scaling with n . When $n \gg r(d + k - r)$, the low-rank parameterization cannot satisfy all constraints.

Note on existential nature. This bound is existential: it guarantees the *existence* of unachievable labelings, not that every labeling below the threshold is achievable. For classification, the margin-based constraints are weaker than exact output matching, so the effective capacity may be higher for benign labelings. The bound is most informative for adversarial or random labelings that lack low-rank structure. \square

D.2. Complete Proof of Theorem 3.7

Proof. We derive the bias-variance decomposition and optimal rank.

Preliminaries. The bias-variance decomposition holds exactly for squared loss $\mathcal{L}(y, \hat{y}) = (y - \hat{y})^2$. For classification with cross-entropy loss, we interpret the decomposition as applying to the underlying regression problem of predicting class probabilities, where the approximation error, estimation error, and noise-induced error terms analogously contribute to excess risk. This interpretation is standard in the statistical learning literature (Hastie et al., 2001) and provides the correct scaling behavior.

Step 1: Bias term (approximation error). Under Assumption 3.6, the best rank- r approximation to the true function f^* has error $\|f^* - f_r^*\|^2 = \mathcal{O}(r^{-2\alpha})$. This is the irreducible bias from restricting to a low-rank model class, independent of the training data.

Step 2: Variance term (estimation error). With $\mathcal{O}(rd)$ effective parameters and n samples (ignoring noise), standard results from statistical learning theory give the estimation error as $\mathcal{O}(\text{complexity}/n) = \mathcal{O}(rd/n)$. This can be derived from Rademacher complexity bounds or metric entropy ar-

guments adapted to low-rank matrices. The variance term captures the error due to finite-sample estimation of the optimal rank- r model.

Step 3: Noise term (label corruption error). With noise rate η , approximately ηn samples have corrupted labels. By Theorem 3.3, the low-rank parameterization becomes overconstrained when the number of samples requiring individual memorization exceeds $O(r(d + k - r))$. When the model has capacity to fit noisy labels, this introduces additional error proportional to the fraction of capacity devoted to noise. The contribution to error from memorized noise is $\mathcal{O}(\eta rd/n)$, reflecting that higher rank and higher noise rate both increase susceptibility to label corruption.

Combining the three terms:

$$\begin{aligned} \mathbb{E}[\text{Error}] &= \underbrace{O(r^{-2\alpha})}_{\text{bias}} + \underbrace{O(rd/n)}_{\text{variance}} + \underbrace{O(\eta rd/n)}_{\text{noise}} \\ &= O(r^{-2\alpha}) + O((1 + \eta)rd/n) \end{aligned} \quad (6)$$

Step 4: Optimization. To find the optimal rank, we differentiate the bound with respect to r . Let the total error be $E(r) = C_1 r^{-2\alpha} + C_2 (1 + \eta)dr/n$ for constants $C_1, C_2 > 0$. Setting $\frac{dE}{dr} = 0$:

$$-2\alpha C_1 r^{-2\alpha-1} + C_2 (1 + \eta)d/n = 0$$

Solving for r :

$$\begin{aligned} r^{2\alpha+1} &= \frac{2\alpha C_1 n}{C_2 (1 + \eta)d} \\ \implies r^* &= O\left(\left(\frac{n}{d(1 + \eta)}\right)^{\frac{1}{2\alpha+1}}\right) \end{aligned} \quad (7)$$

This confirms that optimal rank decreases with noise rate η and increases sublinearly with the ratio n/d . \square

D.3. Complete Proof of Theorem 3.10

Proof. We establish the temporal separation between clean pattern learning and noise memorization.

Step 1: Gradient covariance decomposition. Consider training samples $\{(x_i, \tilde{y}_i)\}_{i=1}^n$ where a fraction η have corrupted labels. The gradient covariance matrix decomposes as:

$$\Sigma = (1 - \eta)\Sigma_{\text{clean}} + \eta\Sigma_{\text{noise}} + \text{cross terms}$$

where Σ_{clean} is the covariance of gradients from clean samples (which share coherent structure) and Σ_{noise} is the covariance from noisy samples (which have incoherent, sample-specific gradients).

Step 2: Spectral structure. For clean samples following a true pattern, gradients align with a low-dimensional subspace. The top singular values of Σ_{clean} are $\sigma_1 \geq \dots \geq$

$\sigma_r = \Omega(\sqrt{(1-\eta)n})$, reflecting the coherent signal structure. For noisy samples, gradients point in diverse directions (since corrupted labels are random), yielding singular values $\sigma_{\text{noise}} = O(\sqrt{\eta})$ that are diffuse across many directions. (In finite samples, the empirical covariance scales proportionally with sample count.)

Step 3: Gradient flow dynamics. Under gradient flow on the LoRA parameters, the update in direction v_i (the i -th singular vector of Σ) evolves as:

$$\frac{d}{dt} \langle \theta, v_i \rangle \propto \sigma_i \langle \theta, v_i \rangle$$

This yields exponential growth: $\langle \theta(t), v_i \rangle \propto e^{\gamma \sigma_i t}$ where γ is the learning rate.

Step 4: Clean learning phase ($t < t^*/2$). Early in training, the dominant directions are those with largest singular values, corresponding to clean patterns. The model’s predictions align with these directions, rapidly reducing loss on clean samples. Since $\sigma_{\text{clean}} \gg \sigma_{\text{noise}}$, clean directions are amplified first.

Step 5: Transition threshold t^* . As training progresses, clean-sample loss approaches zero and the gradient signal from clean samples diminishes. At this point, the residual gradient is dominated by noisy samples. For noise memorization to commence, the amplified noise component must reach the scale of the (now-small) clean residual.

Quantitatively, the noise component grows as $e^{\gamma \sigma_r t} \cdot \sigma_{\text{noise}} \approx e^{\gamma \sigma_r t} \cdot \sqrt{\eta}$. For this to match the clean signal (which is $O(1)$ at initialization), we need:

$$\begin{aligned} e^{\gamma \sigma_r t^*} \cdot \sqrt{\eta} &= \Theta(1) \\ \implies e^{\gamma \sigma_r t^*} &= \Theta(1/\sqrt{\eta}) \end{aligned} \quad (8)$$

Taking logarithms:

$$t^* = \mathcal{O} \left(\frac{1}{\gamma \sigma_r} \log \left(\frac{1}{\eta} \right) \right)$$

where the $\log(1/\eta)$ factor arises from the exponential dynamics and the signal-to-noise ratio determined by η .

Step 6: Noise learning phase ($t > 2t^*$). Beyond t^* , continued training fits the residual loss, which is dominated by noisy samples. New singular value directions emerge as the model allocates capacity to memorize individual corrupted labels. This phase is characterized by decreasing loss on noisy samples while clean sample performance saturates. \square

E. Additional Experimental Details

E.1. LoRA Configuration

We apply LoRA to the query and value projection matrices in each transformer layer:

- Target modules: q-proj, v-proj
- LoRA alpha: 16 (for both r_L and r_H adapters)
- LoRA dropout: 0.1
- Initialization: Kaiming uniform for A , zeros for B

E.2. Complete Training Hyperparameters

Table 7. Complete hyperparameter settings for all experiments.

Hyperparameter	NLP	Vision
Base model	DistilBERT-base	CNN (3-layer)
Max seq length	128	—
Image size	—	32×32
Learning rate	2×10^{-5}	1×10^{-4}
LR scheduler	Linear + decay	Cosine
Warmup steps	500	0
Batch size	32	64
Epochs (Phase 1)	10	20
Epochs (Phase 4)	5	10
Optimizer	AdamW	AdamW
β_1, β_2	0.9, 0.999	0.9, 0.999
Weight decay	0.01	0.01
Gradient clipping	1.0	1.0
LoRA r_L	4	4
LoRA r_H	16	16
LoRA α	16	16
LoRA dropout	0.1	0.1

E.3. Computational Resources

All experiments were conducted on a single workstation with 36GB RAM, demonstrating that RACT is practical without specialized compute infrastructure. LoRA’s parameter efficiency enables training both adapters with modest memory requirements.

E.4. Random Seeds

We use the following seeds for multi-seed experiments:

- Primary seeds: 42, 123, 456
- Additional seeds for vision: 789, 1024

Results are reported as mean \pm standard deviation across available seeds.